NANO LETTERS
Letter
Cite This: Nano Lett. 2018, 18, 1290−1295
pubs.acs.org/NanoLett

Measuring Microtubule Supertwist and Defects by Three-Dimensional-Force-Clamp Tracking of Single Kinesin-1 Motors

Michael Bugiel,[†] Aniruddha Mitra,[‡,¶] Salvatore Girardo,[§] Stefan Diez,[‡,¶] and Erik Schäffer*[,†]

[†]Eberhard Karls Universität Tübingen, ZMBP, Auf der Morgenstelle 32, 72076 Tübingen, Germany

[‡]Technische Universität Dresden, B CUBE − Center for Molecular Bioengineering and Center for Advancing Electronics Dresden, Arnoldstrasse 18, 01307 Dresden, Germany

[¶]Max Planck Institute of Molecular Cell Biology and Genetics, Pfotenhauerstrasse 108, 01307 Dresden, Germany

[§]Technische Universität Dresden, BIOTEC − Center for Molecular and Cellular Bioengineering, Tatzberg 47/49, 01307 Dresden, Germany

Supporting Information

ABSTRACT: Three-dimensional (3D) nanometer tracking of single biomolecules provides important information about their biological function. However, existing microscopy approaches often have only limited spatial or temporal precision and do not allow the application of defined loads. Here, we developed and applied a high-precision 3D-optical-tweezers force clamp to track in vitro the 3D motion of single kinesin-1 motor proteins along microtubules. To provide the motors with unimpeded access to the whole microtubule lattice, we mounted the microtubules on topographic surface features generated by UV-nanoimprint lithography. Because kinesin-1 motors processively move along individual protofilaments, we could determine the number of protofilaments the microtubules were composed of by measuring the helical pitches of motor movement on supertwisted microtubules. Moreover, we were able to identify defects in microtubules, most likely arising from local changes in the protofilament number. While it is hypothesized that microtubule supertwist and defects can severely influence the function of motors and other microtubule-associated proteins, the presented method allows for the first time to fully map the microtubule lattice in situ. This mapping allows the correlation of motor-filament interactions with the microtubule fine-structure. With the additional ability to apply loads, we expect our 3D-optical-tweezers force clamp to become a valuable tool for obtaining a wide range of information from other biological systems, inaccessible by two-dimensional and/or ensemble measurements.

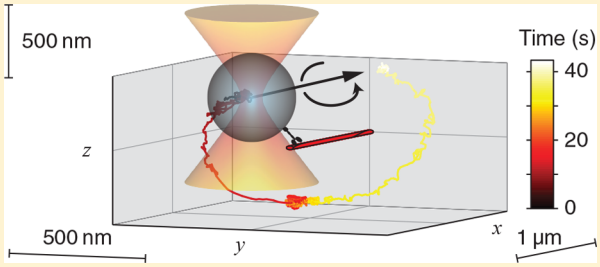

KEYWORDS: *Optical tweezers, force clamp, 3D tracking, single molecule, kinesin, microtubule*

High-precision three-dimensional (3D) tracking is of great interest for investigating biological processes, both in vivo as well as in vitro, providing valuable information that is often inaccessible in conventional microscopy. Approaches with 3D tracking capability include among others confocal imaging,[1−4] defocused imaging,[5−9] the intensity decay of an evanescent field,[10,11] fluorescence−interference contrast (FLIC) microscopy,[12] interference reflection microscopy (IRM, sometimes denoted as iSCAT),[13,14] imaging of split images, separated by a beam splitter,[15] a wedge prism in the back-focal plane,[16] or a special set of mirrors known as Parallax.[17,18] Live-cell 3D superresolution imaging achieves a resolution of 30−50 nm with a 1 Hz bandwidth.[19] Live-cell 3D tracking of single fluorescent emitters typically achieves a 3D precision of several tens of nanometers[20,21] while defocused imaging achieved below 10 nm precision on fixed test samples.[4] Recently, live-cell 3D tracking of 260 nm-diameter fluorescent microspheres reached an axial precision of 20 nm.[22] Although many methods exist for 3D tracking with a precision approaching molecular dimensions, none have the possibility to simultaneously apply forces.

Optical tweezers are versatile tools to apply force, manipulate, and track single molecules with molecular precision.[23,24] Within a certain range, an optical trap is a 3D Hookian spring: forces exerted on dielectric nano-objects are proportional to displacements. The proportionality constant, the spring constant, is called "trap stiffness", which can be determined by calibration procedures in 3D.[25,26] In a force clamp, the relative displacement, and therefore the applied force, of the trapped particle from the trap center is kept constant by a feedback.[27] Under constant applied loads, the motion of single molecules can be tracked with nanometer precision over long distances exceeding 10 μm, potentially in all dimensions. However, common force-clamp approaches use at

Received: November 24, 2017
Revised: January 26, 2018
Published: January 30, 2018

DOI: 10.1021/acs.nanolett.7b04971
Nano Lett. 2018, 18, 1290−1295

most two lateral dimensions, despite the general possibility of optical tweezers to measure displacements and forces in 3D.[27]

Motor proteins are prominent objects of interest for 3D single-molecule experiments. They transduce chemical energy from adenosine triphosphate (ATP) hydrolysis to mechanical motion along cytoskeletal filaments. For example, members of the superfamily of kinesin motors move processively along cytoskeletal microtubules.[28,29] Microtubules are built of linear chains, composed of α/β-tubulin dimers, called protofilaments that bind laterally to each other with an offset of about 1 nm to form a hollow cylinder, the microtubule. Microtubules in vivo mostly have 13 protofilaments and are not supertwisted.[30] For 13 protofilaments, the accumulated lateral offset between tubulin dimers amounts to about 12 nm or the size of three tubulin monomers resulting in a so-called 3-start helix. With a different protofilament number, a microtubule is supertwisted and protofilaments are not parallel to the microtubule axis but rotated and follow a helical path around it.[31] According to this lattice rotation model, the pitch of this helix, called supertwist pitch, depends on the protofilament number in the microtubule.[32,33] Because the microtubule structure is highly polymorphic, the protofilament number, both in vivo and in vitro, can vary between 8 and 20 with microtubule structures corresponding to 2-, 3-, and 4-start helices.[31,34−36] The in vitro composition sensitively depends on the preparation[35,37] and affects the behavior of microtubule-associated proteins and molecular motors.[36] However, in situ determination of the protofilament number is difficult. Conventional kinesin (kinesin-1) is generally accepted to follow the protofilament axis.[37] Thus, 3D helical motion of kinesin-1 on microtubules provides information about the supertwist and microtubule composition.

Here, we describe an approach of a 3D optical-tweezers-based force clamp that is able to follow the motion of single kinesin-1 motors in all three dimensions (Figure 1). For 3D tracking, the clamp employs a piezo tilt mirror and a piezo translation stage for the lateral and axial directions, respectively. Important for a high precision in particular in the axial direction is a trapping laser with a high power stability and a stable setup with a low amount of drift and instrument noise. Using microstructured surfaces with topographical features, we suspended microtubules for free 3D access to microsphere-coupled, single motor proteins. Tracking the motion of these motors in 3D, we found either straight or helical tracks depending on the supertwist of the microtubules. Sudden changes in the movement of the motors were indicative of local defects in the microtubule. The ability to detect the 3D motion of individual molecules with such high precision opens up new possibilities for single-molecule force spectroscopy.

Our 3D force clamp is composed of a single-beam optical trap using an infrared laser with millikelvin-precision temperature control of the trapping objective and near Ångström 3D tracking precision in surface-coupled assays described in detail by Mahamdeh et al.[38,39] For the 3D assay, 3D calibration procedures of back focal plane detection via a quadrant photo diode (QPD) utilizing power spectral density analysis combined with a drag-force method of a trapped microsphere's motion were used as described previously.[25,26] The detailed implementation of a 2D and 3D optical tweezers force-clamp, their tuning and other issues are described in detail in Bugiel et al.[27] The 3D force clamp has already been used to apply various constant 3D loads in DNA[40] and kinesin experiments,[41,42] limited by the proximity of a nearby surface essentially

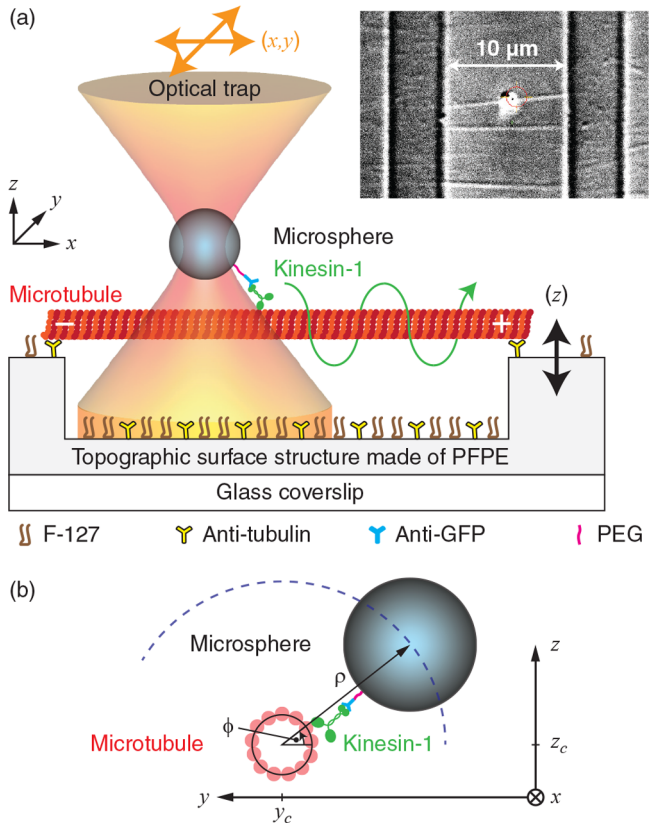

Figure 1. Schematic and geometry of the 3D assay. (a) A 3D kinesin-motor-protein stepping assay using a 3D optical-tweezers force clamp. Microtubules suspended on topographic, nanoimprinted structures provide free access of kinesin-coated microspheres. Inset: Differential interference contrast image of surface structures, microtubules, and a microsphere. (b) Definition of the 3D assay's geometry. The angular and radial position of the microsphere center, ϕ and ρ, respectively, were calculated from the microtubule center coordinates (y_c, z_c) based on a circular fit to the projection of the helical path of the microsphere center around the microtubule (blue dashed line). Both schematics are not to scale.

restricting the motion to 2D. To ensure a high precision and accuracy of tracking in particular in the vertical z-direction, the trapping laser power and the temperature need to be stable (Supporting Information S1). In addition, the fidelity of the optical trap should not depend on position. During the feedback-based force-clamp tracking, the trap position was changed up to 7 μm in the lateral and 1 μm in the axial direction using the piezo tilt mirror and piezo translation stage, respectively. We ensured that the fidelity of the trap characterized by its trap stiffness and displacement sensitivity in 3D did not change more than about 10% over that range (Figure S1, Supporting Information S1). Thus, overall we reduced instrumental noise much below the intrinsic Brownian motion of the trapped microspheres and the biomolecules of interest.

For 3D experiments, full access to the whole microtubule is required (Figure 1a). In 2D experiments, microtubules are usually immobilized on planar surfaces. In common 3D assays, microtubules are suspended on immobilized or optically trapped microspheres[8,43,44] or topographical surface structures of various kinds.[18,45] Here, we used microstructures on coverslips made of perfluoropolyether (PFPE)[46,47] that were fabricated using ultraviolet nanoimprint lithography (UV-

DOI: 10.1021/acs.nanolett.7b04971
Nano Lett. 2018, 18, 1290−1295

NIL,[48] Supporting Information S2). We used PFPE because it has a refractive index close to that of water minimizing trapping artifacts at the edges of the structures. The structures consisted of a repetitive pattern of ridges (2 or 5 μm wide) and valleys (10 μm wide, Figure 1a) on top of an underlying residual layer (Figure S2). The depth of the valleys was 1.4 μm providing sufficient room to accommodate 590 nm-diameter microspheres underneath a suspended microtubule. We used taxol-stabilized microtubules and the truncated rat kinesin-1 *rkin430* coupled to polystyrene microspheres preserving motor functionality under single-molecule conditions[41,49,50] (Supporting Information S3 and S4). We used kinesin-1 because it is known to follow the protofilament axis on a microtubule.[12,37,41] Therefore, tracking the motion of a single kinesin-1 enabled us to measure the supertwist of protofilaments around the microtubule axis. For this purpose, microspheres coated with single motors were placed on top of a freely suspended microtubule and the 3D force clamp was engaged with a zero-force set point in all dimensions. In this manner, no net load was applied to the single motor during translocations. The lateral directions were defined as x and y with the microtubule oriented along the x-axis and the vertical direction denoted as z (Figure 1). The angular and radial position, ϕ and ρ, respectively, were defined by a cylindrical coordinate system relative to the microtubule axis (Supporting Information S5). To track the motor with high precision, the absolute 3D position of the microsphere in these stepping assays was then recorded as a function of time.[27]

In the absence of loads, we tested the performance of the 3D force clamp using infrequent pauses present in the motility of microspheres driven by single kinesin-1 motors[41] (Figure 2). For pausing motors, the 3D trajectory of the microsphere center was curved around the microtubule axis (see xz-projection in Figure 2a) expected for the tethered motion around the suspended microtubule and consistent with similar measurements by Jeney et al. in a static trap.[51] The average root-mean-squared (rms) noise of 12 such measurements in x, y, and z were 13, 18, and 18 nm, respectively, measured as the standard deviation of median-filtered data with 8 Hz bandwidth over the pause duration lasting about 3−70 s (Figure 2a). These rms values were similar to the rms noise $\sigma_{rms} = \sqrt{k_B T/\kappa}$ expected for an unbound microsphere in a static trap, where k_B is the Boltzmann constant, T is the absolute temperature, and κ is the trap stiffness. Thus, the measurement is primarily limited by Brownian motion. Note that these rms values describe the tracking precision with an engaged force clamp and not the localization precision. The instrumental localization precision is better than 1 Å in 3D for averaging times of 0.01−1 s.[38] The average rms noise of the angle ϕ was 3.6° (Figure 2b) potentially allowing to detect angular protofilament-switching steps of 360°/13 ≈ 28° with a signal-to-noise ratio of ≈9. The average rms noise of the radial position ρ was 14 nm. The average rms noise of the forces were about 0.27 pN (x and y) and 0.13 pN (z, Figure 2c), providing subpiconewton resolution. The noise in the z-direction was less because the motion was restricted by the attachment tether. Because averaging of Brownian motion improves precision for short times until ultimately instrumental drift becomes limiting, we determined the tracking precision by means of the Allan deviation as a function of the averaging time[38,52] (Figure 2d). Over 3 orders of magnitude of bandwidth (≈0.2−200 ms), the 3D positional and angular tracking precision was better than 10 nm and 2°, respectively. Thus, 3D tracking of active motors is feasible with high spatiotemporal precision.

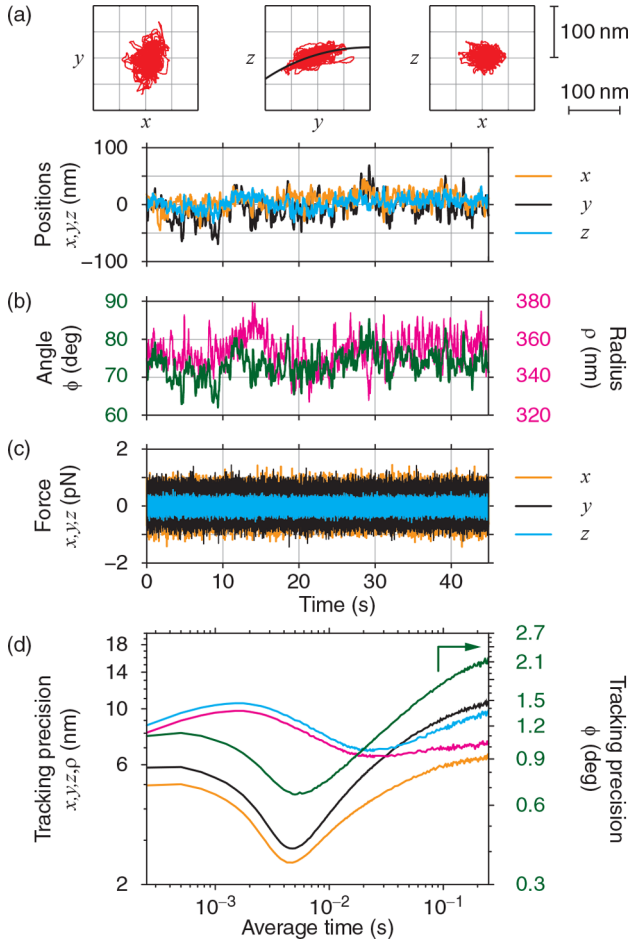

Figure 2. Tracking precision of the 3D force clamp. (a) Three-dimensional plot of x, y, and z-position, with xy, yz, and xz-projections of a stationary kinesin-1-bound 590 nm-diameter polystyrene microsphere on a suspended microtubule. The sampling rate was 4 kHz, filtered down to 8 Hz with a running median filter; the feedback rate was 1 kHz. The data in the yz-projection were fitted with a circle (black line) to extract the angular and radial positions ϕ and ρ. (b) Angle ϕ (green line, left axis) and radius ρ (magenta line, right axis) as a function of time. (c) Clamped force (without additional filtering) as a function of time. The trap stiffnesses were $\kappa_x = \kappa_y = 0.036$ pN/nm, $\kappa_z = 0.006$ pN/nm. (d) Precision of x, y, z, ϕ and ρ as a function of averaging time τ (Allan deviation).

When we tracked single, motile kinesin-1 motors, we observed either straight or unidirectional helical paths (Figure 3a,b). Helical traces had an average radius of 370 ± 20 nm (N = 32, SEM) consistent with the expected value based on the microsphere and microtubule radius and motor-linker length of about 350 nm (Supporting Information S5). The good agreement indicates that microtubules do not fluctuate significantly and are rigidly fixed on the topographic features. The helicity is defined by either increasing or decreasing values of ϕ corresponding to a left- or right-handed rotation and supertwist, respectively. We observed no discrete angular steps in the traces that would correspond to protofilament switching of kinesin-1. Rotational pitches were calculated from the angular slope as a function of forward position (Supporting Information S5). A histogram of the reciprocal pitches of 156 measured traces recorded on 93 distinct microtubules, is shown

DOI: 10.1021/acs.nanolett.7b04971
Nano Lett. 2018, 18, 1290−1295

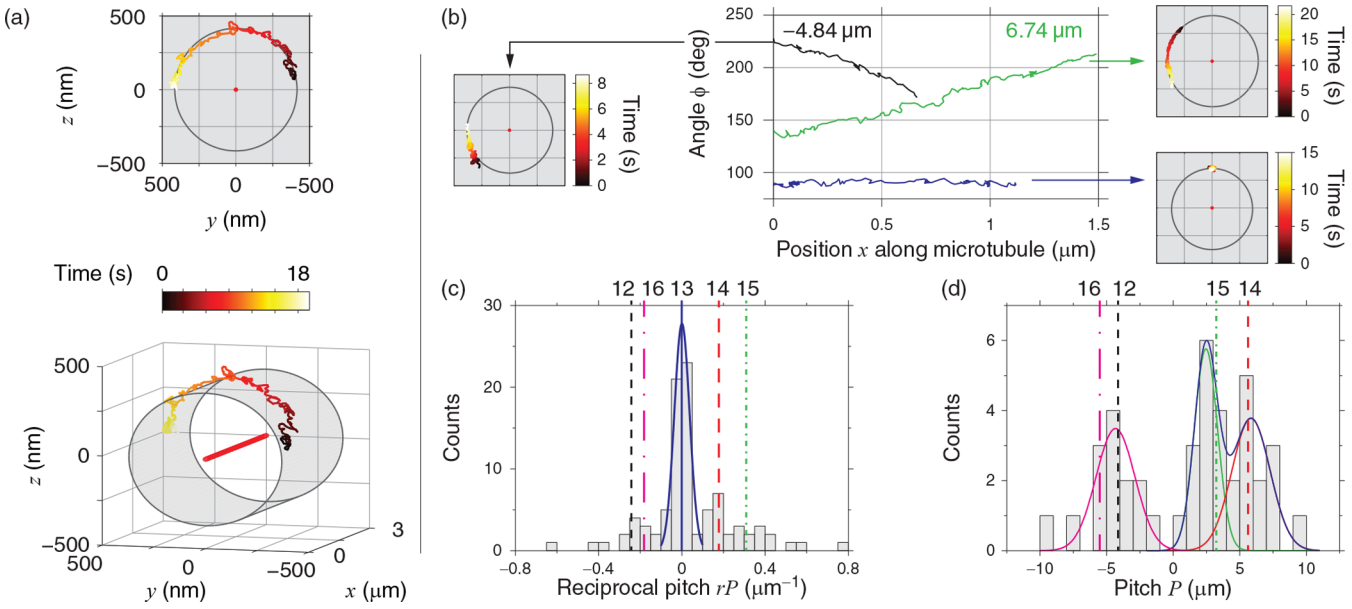

Figure 3. The 3D kinesin-1 tracks and microtubule pitches. (a) The 2D and 3D plots of a helical kinesin-1 path around the microtubule (red center dot or line). (b) Three exemplary angular traces plotted as a function of the *x*-position along the microtubule showing left-handed (green), straight (blue), and right-handed angular motion (black), respectively. For the left- and right-handed motion, pitches are given. Corresponding insets show the *zy*-projections of the microsphere positions over a range of 1 × 1 μm^2, including circular fits on which the angle ϕ is based. (c) Histogram of reciprocal pitches. Gaussian (blue) fitted to reciprocal pitches of −0.1···0.1 μm^{-1} corresponding to straight-protofilament microtubules. Vertical lines indicate expected values for reciprocal pitches[33] of supertwisted microtubules with 12−16 protofilaments. (d) Histogram of pitches excluding straight-protofilament microtubules with multiple Gaussian fits.

Table 1. Microtubule Pitch and Composition (Mean ± SEM)

protofilament number	12	16	13	14	15
theoretical pitch (μm)[32,33]	−4.1	−5.5	∞	5.6	3.2
measured pitch (μm)	−4.3 ± 0.3		$(0.001 \pm 0.004)^{-1}$	5.8 ± 0.7	2.5 ± 0.3
relative amount (%)	15 ± 4		56 ± 5	15 ± 2	14 ± 2

in Figure 3c. The reciprocal pitch was useful because the pitch diverges for straight, 13-protofilament microtubules. Therefore, we defined zero values for straight 3D trajectories with pitches >10 μm[37] corresponding to nonsupertwisted microtubules. Excluding straight traces, the distribution of pitches of supertwisted microtubules (Figure 3c) showed discrete peaks close to the theoretical[33] and literature[12,31,37] values for microtubules with 12−16 protofilaments (Table 1). We could not distinguish pitches with protofilament numbers of 12 and 16. In addition, we determined the relative amount of the different microtubule structures based on the area underneath the Gaussian fits, whereby the relative number of straight microtubules was based on the 10 μm pitch threshold. The broad composition with respect to the protofilament numbers is consistent with previous measurements.[37]

Interestingly, some motor traces measured with the 3D force clamp contained large, localized abrupt changes in the angular slope (Figure 4a). We interpret these events as defects in the microtubule[53] accompanied by possible changes in the protofilament number (Figure 4b). Such changes in protofilament number have been observed in microtubules in vitro and in vivo by electron microscopy.[54] Out of our 156 traces recorded on 93 different microtubules, 22 traces recorded on 18 different microtubules contained a discontinuous change or switch in the angular slope. On the basis of the overall microtubule length of the concatenated 156 traces of 90 μm, the length−frequency of switches was 0.24 ± 0.05 μm^{-1}. This

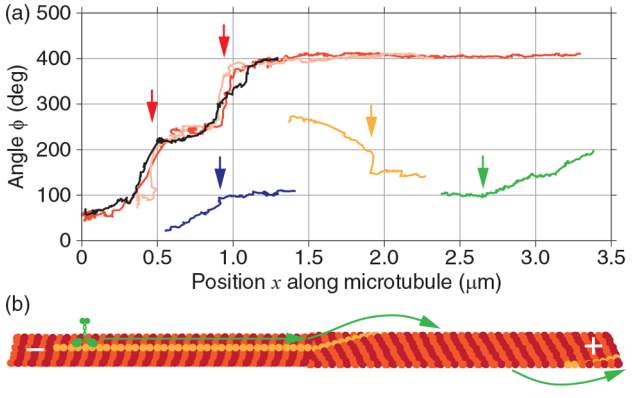

Figure 4. Microtubule defects. (a) Exemplary angular traces plotted as a function of the *x*-position along the microtubule. Traces show sudden changes in angular slopes indicated by arrows. The two red traces in the upper left-hand corner were recorded on the same microtubule. Traces are offset for clarity. (b) Schematic of a microtubule with a defect in the middle: a change in the protofilament number and supertwist causes a motor (green) to change from a straight to a helical path (orange marked tubulin dimers).

value is in excellent agreement with the literature value of 0.25 μm^{-1}[54] supporting the hypothesis that abrupt changes in angular slope correspond to changes in the protofilament number. Thus, on average we expect one change in protofilament number for every 4 μm of microtubule length.

DOI: 10.1021/acs.nanolett.7b04971
Nano Lett. 2018, 18, 1290−1295

Because suspended microtubules had at least a length of 10 μm, we expect on average to have at least two such changes on every suspended microtubule tested. However, because the run length of kinesin-1 is only about 1 μm (Supporting Information S4), not every trace contained such changes. Rotational pitches of these microtubules were determined by analyzing only the longest, constant-slope section of the angular traces. Out of the 22 traces, 12 traces recorded on 8 different microtubules had switches associated with large angular slopes (Figure 4a). Next to these regions extending up to 260 nm in length (about 32 tubulin dimers), the angular slope corresponded to a slope expected for a certain protofilament number and 3-start helix. The large slopes are consistent with 2- and 4-start helix structures or could correspond to transition zones between different microtubule lattices, in which defect-induced strain causes a large supertwist. Furthermore, we observed that angular-slope-change events occurred at approximately the same position when recording traces repeatedly on the same microtubule (e.g., the traces marked with red arrows in Figure 4a) indicating that these positions are not tracking artifacts, for example, through a force bias, but indeed microtubule defects with a well-defined protofilament structure that is tracked by the motor. Such a well-defined structure would also be expected from the stereospecific binding of tubulin. Also, the abrupt-angle-change events are likely not due to short detachment events of the motors as described by Schneider et al.[55] as we did not see forward/backward jumps associated with the abrupt angle changes. After detachment, the force clamp quickly moves the microsphere away from the microtubule preventing reattachment. In addition, rotational diffusion of the trapped microsphere causes the motor to get out of reach of the microtubule within milliseconds. Initial attachment usually occurred on the second time scale. Together, detachment-reattachment events appear to be unlikely.

As controls, we performed multimotor gliding motility assays with speckled microtubules using fluorescence interference contrast microscopy, FLIC,[56] (Supporting Information S6). Consistent with our 3D single-motor measurements, we observed distinct rotational pitches of supertwisted microtubules being propelled by multiple surface-immobilized kinesin-1 motors (Figure S3). However, even for the same preparation of microtubules we observed differences in pitch distributions between gliding and stepping assays (Figure S3c), which we attribute to the following reason: In gliding assays, we always probe the entirety of the microtubule, that is, its full length of more than 1 μm and all protofilaments, meaning we average over all different supertwists arising from changes in the number of protofilaments due to defects. Thus, for example, if a microtubule had segments of both untwisted 13 and supertwisted 12 or 14 protofilaments, the average pitch would be larger compared to a pure 12- or 14-protofilament microtubule. In stepping assays, we always probe short segments of the microtubule on only selected protofilaments. Hence, we obtained unbiased data. While the multimotor-gliding-assay approach is advantageous in that it allows the measurement of multiple full rotations, even for motors with short run length like kinesin-1, we note that it does not allow the identification of local changes in protofilament number.

In summary, we have shown that our experimental approach is suited to track the 3D motion of kinesin-1-coated microspheres on suspended microtubules. Using the protofilament-tracking kinesin-1 with our 3D-force-clamp method enabled us to directly measure the pitch and handedness of supertwisted microtubules. In addition, we could infer the protofilament number of microtubules and, due to our much better angular tracking precision amplified by the microsphere compared to fluorescent-based assays—observe occasional defects in the microtubules. These defects were not visible in multimotor gliding assays that can provide in situ information on the microtubule lattice.[12,37,56] In our optical tweezers assay, repeated experiments starting at approximately the same position on the microtubule can be performed, which is impossible in fluorescence microscopy assays. We used this advantage not only to localize defects repeatedly on the same microtubule,[57] but also to detect the nature of the defect such as a switch in protofilament number. Our observed occasional phases of motor pausing might also refer to defects in the microtubule as suggested by previous multimotor measurements.[57] Those defects could be investigated in more detail using annealed microtubules with different protofilament numbers as done by Gramlich et al.[58] Apart from detecting microtubule defects, the optical tweezers allow to apply forces, for example, to measure load-dependent rates for molecular motors not limited by a 2D geometry.[41] In a static trap and the 3D assay, we could apply piconewton loads on the motors on freely suspended microtubules and confirmed the kinesin-1 stall force of 5−6 pN and 8 nm steps (Figure S4). While we achieved a tracking precision of about 10 nm without force, the tracking precision can be further improved by working with a larger trap stiffness or by applying loads with the force clamp.[27] The 3D force clamp could be used to investigate the 3D motion of other cytoskeletal motor proteins from the kinesin and dynein family that have been shown to switch protofilaments.[8,16,41,44,56,59,60] In general, the 3D force clamp provides a new tool for high-precision, single-molecule in vitro tracking assays and should in principle be also applicable to in vivo systems.

■ ASSOCIATED CONTENT

Supporting Information

The Supporting Information is available free of charge on the ACS Publications website at DOI: 10.1021/acs.nanolett.7b04971.

Trap fidelity; micropatterned glass coverslip fabrication; 3D-force-clamp assays; motor speed and run length; coordinate system for tracking; gliding assays; applying loads to motors walking on freely suspended microtubules (PDF)

■ AUTHOR INFORMATION

Corresponding Author

*E-mail: erik.schaeffer@uni-tuebingen.de. Phone: +49 (0)7071 2978831. Fax: +49 (0)7071 295042.

ORCID

Stefan Diez: 0000-0002-0750-8515

Erik Schäffer: 0000-0001-7876-085X

Notes

The authors declare no competing financial interest.

■ ACKNOWLEDGMENTS

M.B. thanks the Rosa Luxemburg Foundation for a Ph.D. fellowship. This work was supported by the European Research Council (ERC Starting Grant 2010, Nanomech 260875), the German Research Foundation (Cluster of Excellence Center

DOI: 10.1021/acs.nanolett.7b04971
Nano Lett. 2018, 18, 1290−1295

for Advancing Electronics Dresden), the Technische Universität Dresden, and the Eberhard Karls Universität Tübingen. We thank the BIOTEC/CRTD Microstructure Facility of the Technische Universität Dresden (partly funded by the State of Saxony and the European Fund for Regional Development - EFRE) for the production of the patterned glass coverslips.

REFERENCES

(1) Török, P.; Wilson, T. *Opt. Commun.* **1997**, *137*, 127−135.
(2) Dinsmore, A. D.; Weeks, E. R.; Prasad, V.; Levitt, A. C.; Weitz, D. A. *Appl. Opt.* **2001**, *40*, 4152−4159.
(3) Levi, V.; Ruan, Q.; Gratton, E. *Biophys. J.* **2005**, *88*, 2919−2928.
(4) Gardini, L.; Capitanio, M.; Pavone, F. S. *Sci. Rep.* **2015**, *5*, 16088.
(5) Speidel, M.; Jonáš, A.; Florin, E.-L. *Opt. Lett.* **2003**, *28*, 69−71.
(6) Prabhat, P.; Ram, S.; Ward, E. S.; Ober, R. J. *Proc. SPIE* **2006**, *6090*, 60900L.
(7) Otto, O.; Gornall, J.; Stober, G.; Czerwinski, F.; Seidel, R.; Keyser, U. *J. Opt.* **2011**, *13*, 044011.
(8) Can, S.; Dewitt, M. A.; Yildiz, A. *eLife* **2014**, *3*, 1−12.
(9) Huhle, A.; Klaue, D.; Brutzer, H.; Daldrop, P.; Joo, S.; Otto, O.; Keyser, U. F.; Seidel, R. *Nat. Commun.* **2015**, *6*, 5885.
(10) Singh-Zocchi, M.; Dixit, S.; Ivanov, V.; Zocchi, G. *Proc. Natl. Acad. Sci. U. S. A.* **2003**, *100*, 7605−7610.
(11) Brutzer, H.; Schwarz, F. W.; Seidel, R. *Nano Lett.* **2012**, *12*, 473−478.
(12) Nitzsche, B.; Ruhnow, F.; Diez, S. *Nat. Nanotechnol.* **2008**, *3*, 552−556.
(13) Curtis, A. S. G. *J. Cell Biol.* **1964**, *20*, 199−215.
(14) Spindler, S.; Ehrig, J.; König, K.; Nowak, T.; Piliarik, M.; Stein, H. E.; Taylor, R. W.; Garanger, E.; Lecommandoux, S.; Alves, I. D.; Sandoghdar, V. *J. Phys. D: Appl. Phys.* **2016**, *49*, 274002.
(15) Toprak, E.; Balci, H.; Blehm, B. H.; Selvin, P. R. *Nano Lett.* **2007**, *7*, 2043−2045.
(16) Yajima, J.; Mizutani, K.; Nishizaka, T. *Nat. Struct. Mol. Biol.* **2008**, *15*, 1119−1121.
(17) Sun, Y.; McKenna, J. D.; Murray, J. M.; Ostap, E. M.; Goldman, Y. E. *Nano Lett.* **2009**, *9*, 2676−2682.
(18) Sun, Y.; Sato, O.; Ruhnow, F.; Arsenault, M. E.; Ikebe, M.; Goldman, Y. E. *Nat. Struct. Mol. Biol.* **2010**, *17*, 485−491.
(19) Jones, S. A.; Shim, S.-H.; He, J.; Zhuang, X. *Nat. Methods* **2011**, *8*, 499−505.
(20) Pavani, S. R. P.; Thompson, M. A.; Biteen, J. S.; Lord, S. J.; Liu, N.; Twieg, R. J.; Piestun, R.; Moerner, W. E. *Proc. Natl. Acad. Sci. U. S. A.* **2009**, *106*, 2995−2999.
(21) Wells, N. P.; Lessard, G. A.; Goodwin, P. M.; Phipps, M. E.; Cutler, P. J.; Lidke, D. S.; Wilson, B. S.; Werner, J. H. *Nano Lett.* **2010**, *10*, 4732−4737.
(22) Verdeny-Vilanova, I.; Wehnekamp, F.; Mohan, N.; Álvarez, Á. S.; Borbely, J. S.; Otterstrom, J. J.; Lamb, D. C.; Lakadamyali, M. *J. Cell Sci.* **2017**, *130*, 1904.
(23) Ashkin, A.; Dziedzic, J. M.; Bjorkholm, J. E.; Chu, S. *Opt. Lett.* **1986**, *11*, 288−290.
(24) Gennerich, A. *Optical Tweezers: Methods and Protocols*; Methods Mol. Biol.; Springer: New York, 2017; Vol. *1486*.
(25) Tolić-Nørrelykke, S. F.; Schäffer, E.; Howard, J.; Pavone, F. S.; Jülicher, F.; Flyvbjerg, H. *Rev. Sci. Instrum.* **2006**, *77*, 103101.
(26) Schäffer, E.; Nørrelykke, S. F.; Howard, J. *Langmuir* **2007**, *23*, 3654−3665.
(27) Bugiel, M.; Jannasch, A.; Schäffer, E. In *Optical Tweezers: Methods and Protocols*; Gennerich, A., Ed.; Springer Press, 2017; Chapter 5.
(28) Block, S. M.; Goldstein, L. S. B.; Schnapp, B. J. *Nature* **1990**, *348*, 348−352.
(29) Svoboda, K.; Schmidt, C. F.; Schnapp, B. J.; Block, S. M. *Nature* **1993**, *365*, 721−727.
(30) Tilney, L. G.; Bryan, J.; Bush, D. J.; Fujiwara, K.; Mooseker, M. S.; Murphy, D. B.; Snyder, D. H.; et al. *J. Cell Biol.* **1973**, *59*, 267−275.
(31) Howard, J. *Motor Proteins and the Cytoskeleton*; Sinauer Associates: Sunderland, MA, 2001.
(32) Chrétien, D.; Wade, R. H. *Biol. Cell* **1991**, *71*, 161−174.
(33) Wade, R.; Chrétien, D. *J. Struct. Biol.* **1993**, *110*, 1−27.
(34) Unger, E.; Böhm, K.; Vater, W. *Electron Microsc. Rev.* **1990**, *3*, 355−395.
(35) Sui, H.; Downing, K. H. *Structure* **2010**, *18*, 1022−1031.
(36) Brouhard, G. J.; Rice, L. M. *J. Cell Biol.* **2014**, *207*, 323−334.
(37) Ray, S.; Meyhöfer, E.; Milligan, R. A.; Howard, J. *J. Cell Biol.* **1993**, *121*, 1083−1093.
(38) Mahamdeh, M.; Schäffer, E. *Opt. Express* **2009**, *17*, 17190−17199.
(39) Mahamdeh, M.; Campos, C. P.; Schäffer, E. *Opt. Express* **2011**, *19*, 11759−11768.
(40) Ander, M.; Subramaniam, S.; Fahmy, K.; Stewart, A. F.; Schäffer, E. *PLoS Biol.* **2015**, *13*, e1002213.
(41) Bugiel, M.; Böhl, E.; Schäffer, E. *Biophys. J.* **2015**, *108*, 2019−27.
(42) Ramaiya, A.; Roy, B.; Bugiel, M.; Schäffer, E. *Proc. Natl. Acad. Sci. U. S. A.* **2017**, *114*, 201706985.
(43) Oguchi, Y.; Uchimura, S.; Ohki, T.; Mikhailenko, S. V.; Ishiwata, S. *Nat. Cell Biol.* **2011**, *13*, 846−852.
(44) Brunnbauer, M.; Dombi, R.; Ho, T.-H.; Schliwa, M.; Rief, M.; Ökten, Z. *Mol. Cell* **2012**, *46*, 147−158.
(45) Roos, W.; Ulmer, J.; Gräter, S.; Surrey, T.; Spatz, J. P. *Nano Lett.* **2005**, *5*, 2630−2634.
(46) Rolland, J. P.; Van Dam, R. M.; Schorzman, D. A.; Quake, S. R.; DeSimone, J. M. *J. Am. Chem. Soc.* **2004**, *126*, 2322−2323.
(47) Williams, S. S.; Retterer, S.; Lopez, R.; Ruiz, R.; Samulski, E. T.; DeSimone, J. M. *Nano Lett.* **2010**, *10*, 1421−1428.
(48) Austin, M. D.; Ge, H.; Wu, W.; Li, M.; Yu, Z.; Wasserman, S. A. L.; Chou, S. Y.; et al. *Appl. Phys. Lett.* **2004**, *84*, 5299−5301.
(49) Jannasch, A.; Bormuth, V.; Storch, M.; Howard, J.; Schäffer, E. *Biophys. J.* **2013**, *104*, 2456−2464.
(50) Bugiel, M.; Fantana, H.; Bormuth, V.; Trushko, A.; Schiemann, F.; Howard, J.; Schäffer, E.; Jannasch, A. *JBM* **2015**, *2*, 30.
(51) Jeney, S.; Stelzer, E. H. K.; Grubmüller, H.; Florin, E.-L. *ChemPhysChem* **2004**, *5*, 1150−1158.
(52) Czerwinski, F.; Richardson, A. C.; Oddershede, L. B. *Opt. Express* **2009**, *17*, 13255−13269.
(53) Schaap, I. A. T.; de Pablo, P. J.; Schmidt, C. F. *Eur. Biophys. J.* **2004**, *33*, 462−467.
(54) Chrétien, D.; Metoz, F.; Verde, F.; Karsenti, E.; Wade, R. *J. Cell Biol.* **1992**, *117*, 1031−40.
(55) Schneider, R.; Korten, T.; Walter, W. J.; Diez, S. *Biophys. J.* **2015**, *108*, 2249−2257.
(56) Mitra, A.; Ruhnow, F.; Nitzsche, B.; Diez, S. *PLoS One* **2015**, *10*, e0136920.
(57) Liang, W. H.; Li, Q.; Faysal, K. M. R.; King, S. J.; Gopinathan, A.; Xu, J. *Biophys. J.* **2016**, *110*, 2229−2240.
(58) Gramlich, M. W.; Conway, L.; Liang, W. H.; Labastide, J. A.; King, S. J.; Xu, J.; Ross, J. L. *Sci. Rep.* **2017**, *7*, 44290.
(59) Bormuth, V.; Nitzsche, B.; Ruhnow, F.; Mitra, A.; Storch, M.; Rammner, B.; Howard, J.; Diez, S. *Biophys. J.* **2012**, *103*, L04−L06.
(60) Yamaguchi, S.; Saito, K.; Sutoh, M.; Nishizaka, T.; Toyoshima, Y.; Yajima, J. *Biophys. J.* **2015**, *108*, 872−879.

DOI: 10.1021/acs.nanolett.7b04971
Nano Lett. 2018, 18, 1290−1295